AGU PUBLICATIONS

JGR

Journal of Geophysical Research: Atmospheres

RESEARCH ARTICLE
10.1002/2016JD024982

Key Points:
- The impacts of surface heterogeneity on dry PBLs in an urban-rural setting are investigated by using a modified WRF-LES model
- The urban-rural contrasts in roughness length and surface temperature have significant but different impacts on PBL characteristics
- The impacts of urban surface heterogeneity are strongly dependent on the heterogeneity scale

Correspondence to:
T. Sun,
sunting@tsinghua.edu.cn

Citation:
Zhu, X., G. Ni, Z. Cong, T. Sun, and D. Li (2016), Impacts of surface heterogeneity on dry planetary boundary layers in an urban-rural setting, *J. Geophys. Res. Atmos.*, *121*, doi:10.1002/2016JD024982.

Received 27 FEB 2016
Accepted 13 OCT 2016
Accepted article online 15 OCT 2016

Impacts of surface heterogeneity on dry planetary boundary layers in an urban-rural setting

Xiaoliang Zhu[1,2], Guangheng Ni[1], Zhentao Cong[1], Ting Sun[1], and Dan Li[2]

[1]State Key Laboratory of Hydroscience and Engineering, Department of Hydraulic Engineering, Tsinghua University, Beijing, China, [2]Department of Earth and Environment, Boston University, Boston, Massachusetts, USA

Abstract Understanding the impacts of land use and land-cover change such as urbanization is essential in many disciplines. This study investigates the impacts of urban-rural contrasts in terms of momentum roughness length (z_0) and aerodynamic surface temperature (TSK) on dry planetary boundary layers (PBLs) using large-eddy simulations (LES) with the Weather Research and Forecasting (WRF) model. In addition, the impacts of small-scale heterogeneities within urban areas are also examined. The original WRF-LES is modified in order to use prescribed TSK as surface boundary conditions. Numerical simulations are then conducted to examine turbulence characteristics and mesoscale circulations resulting from large-scale urban-rural contrasts as well as small-scale heterogeneities in urban areas. The results indicate that (1) the urban-rural contrasts in z_0 and TSK have significant but different impacts on surface heat fluxes, mesoscale circulations, and the wind and potential temperature profiles. Compared to the case where the whole domain is homogeneous, increases in z_0 and/or TSK in urban areas in the center of domain induce stronger sensible heat fluxes, stronger urban circulations, and weaker inversions at the top of the PBL. (2) When the patch size that characterizes the urban heterogeneity scale is comparable to the size of the whole urban area, the simulated results are strongly dependent on both the heterogeneity scale and the specified surface temperature values. As the patch size decreases, the simulated results become more similar to those over a homogeneous urban surface.

1. Introduction

About 52% of the world's population now resides in urban areas that cover only 0.5% of the Earth's land, which leads to many environmental consequences [*Schneider et al*., 2009; *United Nations, Department of Economic and Social Affairs, Population Division*, 2014]. The urban heat island (UHI) effect is one of the most known impacts of urbanization: the surface temperature and near-surface air temperature of urban areas are typically higher than those of the surrounding rural areas [*Arnfield*, 2003; *Grimmond*, 2007; *Oke*, 1982]. The UHI effect has significant implications for human health, energy use, biodiversity, and regional climate [*Grimm et al*., 2008; *Rizwan et al*., 2008]. Numerous studies have shown that the UHI effect can alter the rainfall pattern and amount at regional scales [*Lowry*, 1998; *Miao et al*., 2011; *Shepherd*, 2005; *Yang et al*., 2014]. Recent studies also show that synergies between UHIs and heat waves can create extremely high heat stresses for urban residents [*Li and Bou-Zeid*, 2013; *Li et al*., 2015; *Li et al*., 2016].

The characteristics of urban surfaces are very different from those of natural surfaces. For example, urban surfaces have high fractions of impervious materials such as asphalt and concrete, which prevent the rain from infiltrating to the soil and reduce the evapotranspiration rate. Another example is that urban surfaces, with buildings and other man-made structures, are usually aerodynamically rougher than natural surfaces such as grassland. These unique characteristics of urban environments often result in higher surface or near-surface air temperature (namely, the UHI effect) and stronger surface heating rate in urban areas, which further affects the planetary boundary layer (PBL) and regional climate.

Much is known about the impacts of land surface heterogeneities on turbulent structures and mixing processes in the PBL, particularly thanks to a powerful research tool of large-eddy simulations (LES). For example, *Liu et al*. [2011] investigated turbulent structures in a convective PBL driven by mosaic-like heterogeneous heating at the ground and concluded that the turbulent kinetic energy is not enhanced unless the heterogeneity scale is large enough. *Kang and Lenschow* [2014] studied the temporal evolution of low-level winds induced by two-dimensional heterogeneous heating and found that stronger mesoscale circulations occurred in the spanwise direction even with a background wind in the streamwise direction than those with

no background wind. *Van Heerwaarden et al*. [2014] documented that the optimal state and transition for the vertically integrated kinetic energy do not occur at a fixed ratio of the heterogeneity size to the PBL height but at a ratio that increases with increasing heterogeneity sizes. There are also many studies specifically examining urban-rural contrasts and their impacts. For example, the contrast between urban and rural areas in terms of surface heating rate is shown to generate organized mesoscale circulations [*Baidya Roy*, 2003; *Hidalgo et al*., 2008a; *Hidalgo et al*., 2008b; *Ryu and Baik*, 2013; *Ryu et al*., 2013], the so-called UHI circulations or urban breeze circulations, which have a direct influence on surface fluxes, the atmospheric flow, temperature profiles, and so on. *Wang* [2009] investigated the influence of UHI circulations induced by urban-rural contrasts in terms of surface sensible heat flux and roughness on flow statistics using LES and found that an isolated UHI could enhance the horizontal velocity variance in the central urban area through the low-level flow convergence. *Zhang et al*. [2014] studied the turbulent characteristics and mesoscale circulations caused by different urban and rural heating rates and found that the UHI intensity has an obvious impact on the spatial distribution of the wind field.

These LES studies often use sensible heat flux as surface boundary conditions. In many numerical models such as the Weather Research and Forecasting (WRF) model [*Chen and Dudhia*, 2001], the surface sensible heat flux (HFX) is calculated following

$$\mathrm{HFX} = \rho c_p \overline{w'\theta'} = \rho c_p C_h U(\theta_s - \theta_a), \tag{1}$$

where ρ is the air density, c_p is the specific heat of air at constant pressure, U is the wind speed at the first atmospheric model level, θ_s is the surface temperature (TSK), θ_a is the air temperature at the first atmospheric model level, C_h is the turbulent transfer coefficient for heat and is computed based on Monin-Obukhov Similarity Theory (MOST) [*Monin and Obukhov*, 1954] as

$$C_h = \frac{\kappa^2}{\left[\ln\left(\frac{z}{z_0}\right) - \psi_m\left(\frac{z}{L}\right)\right]\left[\ln\left(\frac{z}{z_{0T}}\right) - \psi_h\left(\frac{z}{L}\right)\right]}, \tag{2}$$

where κ is the von Kármán constant (≈0.4), z is the height of the first grid level of the atmospheric model, z_0 is the momentum roughness length, z_{0T} is the thermal roughness length, L is the Obukhov length, and ψ_m and ψ_h are the stability correction functions for momentum and heat, respectively. Thus, as sensible heat flux is affected by both surface roughness (z_0) and surface temperature (TSK), representing an urban area by a higher sensible heat flux could not distinguish the dynamic effect (through altering z_0) and thermodynamic effect (through altering TSK) of urbanization. Although these two effects are not independent of each other (i.e., altering z_0 will inevitably change TSK) [*Lee et al*., 2011; *van Heerwaarden and Mellado*, 2016; *Zhao et al*., 2014], studying their impacts separately and jointly motivates our study.

In this study, we focus on the urban-rural contrasts of dynamic and thermodynamic characteristics, which are represented by the roughness length (z_0) and the aerodynamic surface temperature (TSK), respectively. In particular, we aim to assess the relative importance of urban-rural contrasts of dynamic and thermodynamic characteristics in modulating surface sensible heat flux, which further affects boundary layer properties including potential temperature and wind profiles through altering the buoyant production/destruction of turbulent kinetic energy. In addition to the large-scale urban-rural contrast, surface heterogeneities within urban areas due to different surface materials (e.g., grass, asphalt, and concrete) and urban configurations (e.g., industrial zones, high-intensity residential zones, and low-intensity residential zones) may be also important depending on their heterogeneity scales [*Bou-Zeid et al*., 2004, 2007]. However, there has been no study investigating the impact of these small-scale heterogeneities on urban-atmosphere interactions within the context of large-scale urban-rural contrast, which also motivates our study.

To answer these questions, we use the WRF model in LES mode. First, the WRF-LES model is modified so we can specify TSK as surface boundary conditions. Two sets of numerical experiments are then conducted: one is used to investigate the impacts of the dynamic and thermodynamic urban-rural contrasts and the other is used to study the impacts of small-scale surface heterogeneity in urban areas. The paper is organized as follows: the setup of numerical experiments is described in section 2; the simulation results are analyzed and discussed in section 3. The conclusions are presented in section 4.

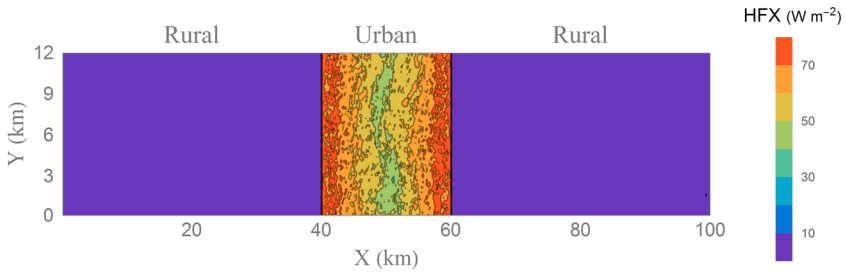

Figure 1. The simulation domain in *x-y* directions. The color shading shows the distribution of sensible heat flux in the default case A0 (see section 2.2) averaged between 18 and 20 h.

2. Numerical Model and Experiments

2.1. Model Description and Configuration

The WRF-LES model has been widely used in previous studies [*Kang and Lenschow*, 2014; *Moeng et al*., 2007; *Talbot et al*., 2012; *Yamaguchi and Feingold*, 2012]. It has proven to be a good simulation tool to investigate convective PBL characteristics under heterogeneous heating conditions [*Kang and Lenschow*, 2014; *Liu et al*., 2011]. In our study, the WRF version 3.5.1 is used. The default surface boundary condition option for WRF-LES is to prescribe sensible heat flux, which is incapable of separating the dynamic and thermodynamic characteristics of urban areas and thus cannot be used to address our research question. Meanwhile, some studies [*Basu et al*., 2008; *Holtslag et al*., 2007] suggest that prescribing surface temperature is a better option than prescribing sensible heat flux under stable conditions. This is because the relation between surface heat flux and the temperature difference between the surface and the atmospheric model is not monotonic under stable conditions. As a result, prescribing surface heat flux could result in two physically sensible values for the friction velocity (and thus two different temperature gradients) and it is hard to determine which of these two values is more appropriate [*Gibbs et al*., 2014]. As shall be seen later, stable conditions occur in our simulations over rural areas due to the inhomogeneous heating rates between urban and rural surfaces, and hence, the WRF-LES model is modified in our study so that surface temperature is prescribed from which sensible heat flux is calculated. The surface layer scheme in the WRF model, which is based on the MOST, is used to calculate the surface heat flux and the friction velocity from prescribed surface temperature and momentum roughness length. Note that MOST is based on many assumptions including horizontal homogeneity, which might be violated in our simulations with large-scale urban-rural contrasts and/or small-scale urban heterogeneities. However, despite being strictly valid for homogeneous flows, MOST has been widely used to provide surface boundary conditions for LES over heterogeneous terrain [*Albertson et al*., 2001; *Huang and Margulis*, 2010; *Miller and Stoll*, 2013; *Stoll and Porté-Agel*, 2006, 2009]. This is partly because there has not been any theory proposed to replace MOST for heterogeneous terrain and also partly because observational evidence shows that many flow statistics over heterogeneous terrain still follow MOST [*Wang et al*., 2014; *Wood et al*., 2010].

From equation (2) it is clear that both the momentum roughness length z_0 and the thermal roughness length z_{0T} can affect the calculation of C_h. In this study, we only prescribe the momentum roughness length z_0 as it is often parameterized as a function of land use. The thermal roughness length z_{0T} is calculated in the surface layer scheme as follows [*Chen and Dudhia*, 2001]:

$$z_{0T} = \frac{1}{\frac{\kappa u_*}{k_a} + \frac{1}{z_l}}, \tag{3}$$

where k_a is the molecular thermal diffusivity of air, u_* is the friction velocity, and z_l (=0.01 m) is molecular sublayer height [*Carlson and Boland*, 1978]. Except for the surface layer scheme, other physics schemes in the WRF-LES model such as microphysics and radiation are all turned off. The model uses a fifth-order scheme for advection in the horizontal direction and a third-order scheme for advection in the vertical direction as suggested by WRF user's guide. The third-order Runge-Kutta scheme is adopted for the time integration with a time step of 1 s. This study uses the 1.5-order turbulent kinetic energy scheme [*Deardorff*, 1980] to compute the subgrid-scale eddy viscosity and eddy diffusivity (diff_opt = 2 and km_opt = 2 in the WRF namelist).

Table 1. An Overview of the First Set of Experiments[a]

Case Name	TSK (K)	z_0 (m)	Wind Speed (m s^{-1})	u_* (m s^{-1})	θ_* (K)	L (m)
W0	304	0.1	0	0.101	−0.090	−8.741
W1	304	0.1	1	0.111	−0.080	−11.26
W5	304	0.1	5	0.279	−0.005	−1041.45
A0	306	0.1	0	0.225	−0.243	−12.52
A1	306	0.1	1	0.186	−0.265	−7.30
A5	306	0.1	5	0.335	−0.136	−59.83
B0	304	0.5	0	0.146	−0.084	−15.83
B1	304	0.5	1	0.154	−0.085	−17.14
B5	304	0.5	5	0.341	−0.001	−11918
AB0	306	0.5	0	0.335	−0.240	−28.95
AB1	306	0.5	1	0.262	−0.216	−17.27
AB5	306	0.5	5	0.420	−0.144	−83.95

[a]The frictional velocity u_*, the potential temperature scale $\theta_* = -HFX/(\rho c_p u_*)$, and the Obukhov length L are averaged from 18 to 20 h over the urban area.

In this study, the simulation domain is 100 km × 12 km in the horizontal directions, as shown in Figure 1, and the number of grid points is 1000 × 120 (i.e., the resolution in both x and y directions is 100 m). The top of the domain is 4 km with 100 levels, and the vertical resolution is about 40 m. The area between 40 km and 60 km is urban land, which has different momentum roughness length and/or surface temperature as compared to the surrounding rural areas (Figure 1). The surface in the entire simulation domain is flat, and thus, the influence of terrain is not considered. The model is initialized with an idealized neutral boundary layer profile, in which the potential temperature is 300 K below 950 m, and there is a strong inversion layer with a potential temperature surge of 50 K km^{-1} from 950 to 1050 m. The potential temperature gradient is 3 K km^{-1} above 1050 m. All cases have the same initial atmospheric conditions. Potential temperature fields in WRF-LES model are perturbed randomly at the first four vertical layers to promote convection. The model is driven by periodic lateral boundary conditions in the horizontal directions.

2.2. Numerical Experiments

In our first set of experiments, we aim to examine the different impacts of dynamic and thermodynamic contrasts between urban and rural areas under different geostrophic wind speed conditions. The dynamic and thermodynamic contrasts are again represented by z_0 and TSK differences, respectively. Over rural areas, the surface temperature and momentum roughness length are set to 304 K and 0.1 m, respectively; while over urban areas they vary in different cases. The values of TSK and momentum roughness length are taken from typical values reported in the literature [*Stull*, 1988]. Table 1 lists all the cases in our first set of experiments and parameters characterizing the stability of the PBL such as the frictional velocity u_*, the potential temperature scale $\theta_* = -HFX/(\rho c_p u_*)$, and the Obukhov length $L = u_*^2/\left(\kappa g \theta_*/\overline{\theta}\right)$ over the urban area, where g is the gravitational acceleration and $\overline{\theta}$ is mean potential temperature. In cases starting with W (i.e., W0, W1, and W5, where the number refers the wind speed in units of m s^{-1} and the wind direction is always along the x direction), the z_0 and TSK of urban areas are set to be the same as the rural areas. In cases starting with A (i.e., A0, A1, and A5), the value of TSK in urban areas varies, while in cases starting with B (i.e., B0, B1, and B5), the value of z_0 in urban areas varies. In cases starting with AB (i.e., AB0, AB1, and AB5), both TSK and z_0 values in urban areas vary. It is noted here that the configuration used in our first set of experiments is different from previous studies using two-dimensional heterogeneous heating [e.g., *Kang and Lenschow*, 2014]. The surface heterogeneity in our configuration is present only in the x direction.

In the second set of experiments (Table 2), the impact of heterogeneities within urban areas is investigated, with a specific focus on the heterogeneity scale. First, the urban area is divided into rectangle patches. Eleven new cases are created, and the number in the case name stands for the number of patches. Then, in each case, the TSK values of different patches are generated by random selection from a Gaussian distribution with the mean of 306 K and the standard deviation of 1 K (Figure 2a). It should be noted that the mean value $\bar{u}$ (and the standard deviation $\overline{\sigma}$) of actual values generated by a random value generator may not be exactly u (and σ) due to insufficient realizations. To avoid significant differences simply caused by insufficient realizations, we ensure that the values of TSK in each case satisfy $|\bar{u} - u| \leq 0.001$ K and $|\overline{\sigma} - \sigma| \leq 0.1$ K. Figure 2b shows an

Table 2. An Overview of the Second Set of Experiments

Case Name	Urban Patch Number	Case Name	Urban Patch Number
A0	1	C80	8 × 10
C4	2 × 2	C100	10 × 10
C8	2 × 4	C300	15 × 20
C16	4 × 4	C1200	30 × 40
C32	4 × 8	C6000	60 × 100
C64	8 × 8	C24000	120 × 200

example of the TSK distribution in case C16. In this set of experiments, the momentum roughness length of urban areas is chosen to be 0.1 m, and there is no geostrophic wind. We note that our approach is idealized and does not necessarily reflect the nature of small-scale urban heterogeneities in the real world. However, this approach does allow us to investigate the impact of such idealized small-scale urban heterogeneities within the context of large-scale urban-rural contrast.

3. Results and Discussion

3.1. The Temporal Evolution of Surface and Boundary Layer Properties

The temporal evolution of sensible heat flux and the boundary layer height in case A0 are presented in Figure 3. Note that the rural areas in the left and right are averaged together since this case is completely symmetrical in the *x* direction. The PBL height is calculated by using the potential temperature gradient method where the PBL height is defined as the level at which the potential temperature gradient becomes larger than 10 K km^{-1}.

As shown in Figure 3, it is clear that the simulation reaches a quasi-steady state after about 20 h. As the air temperature becomes warmer, the sensible heat flux decreases and becomes almost zero or even negative over rural areas. The PBL height over rural areas grows at a constant rate since the beginning of the simulation, while the PBL height over urban areas changes its growth rate after the integration period. The trend is consistent with previous studies using sensible heat flux as surface boundary conditions [*Liu et al.*, 2011], but the rate is different due to a decreasing sensible heat flux in our study. It can also be seen that the averaged PBL height over urban areas is higher than that over rural areas during the integration period, which is caused by the stronger heating rate over urban areas. However, in the later stage, the growth rate of the PBL height over rural areas exceeds that over urban area. Close inspection reveals that this is because the rural boundary layer becomes slightly stable after 40 h so the rural PBL height calculated by the potential temperature gradient method is the sum of stable boundary layer height and the residual layer height. Since developing methods to identify the PBL height is not the emphasis of our study, we will no longer use the PBL height calculated by the potential temperature gradient method but rather directly examine the potential temperature profiles.

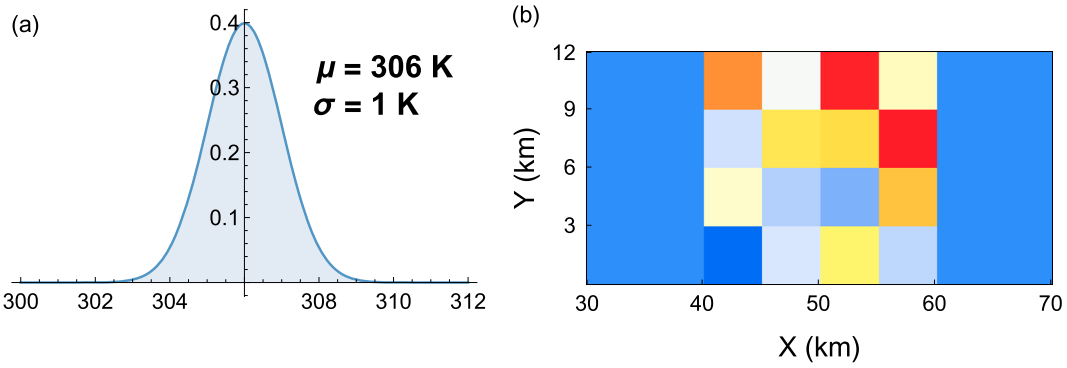

Figure 2. (a) The Gaussian distribution for TSK values in different urban patches. (b) An example of TSK distribution in urban areas: case C16.

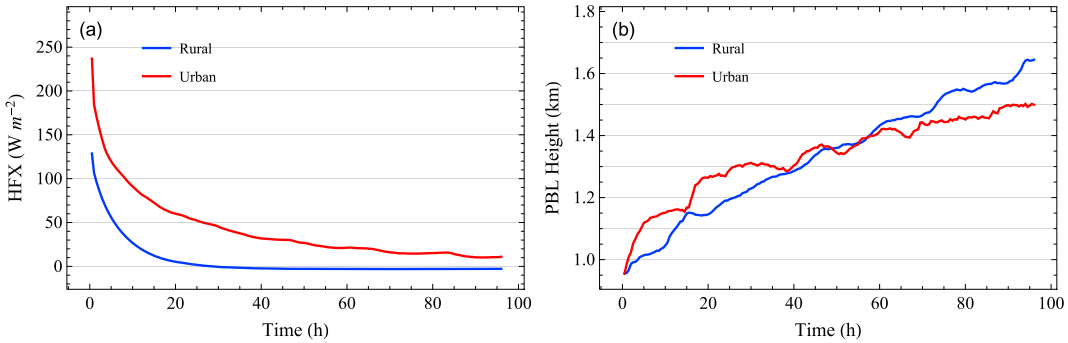

Figure 3. The temporal evolution of averaged sensible heat flux and PBL height for case A0. The red line denotes the urban area; the blue line denotes the rural area.

To further examine the quasi-steady state of our simulations, different kinetic energies are calculated at 120 m above the ground. The total kinetic energy (TTE) and mean kinetic energy (MKE) are defined as

$$\mathrm{TTE} = \frac{1}{2}\left\langle u^2 + v^2 + w^2 \right\rangle, \tag{4}$$

$$\mathrm{MKE} = \frac{1}{2}\left\langle \overline{u}^2 + \overline{v}^2 + \overline{w}^2 \right\rangle, \tag{5}$$

where u, v, and w are the longitudinal, meridional, and vertical velocity components, respectively. The overbars denote the Reynolds averages (represented by the spatial averages in the homogenous y direction). The brackets denote horizontal averages in the x-y plane (i.e., over urban and rural areas). Note that because of

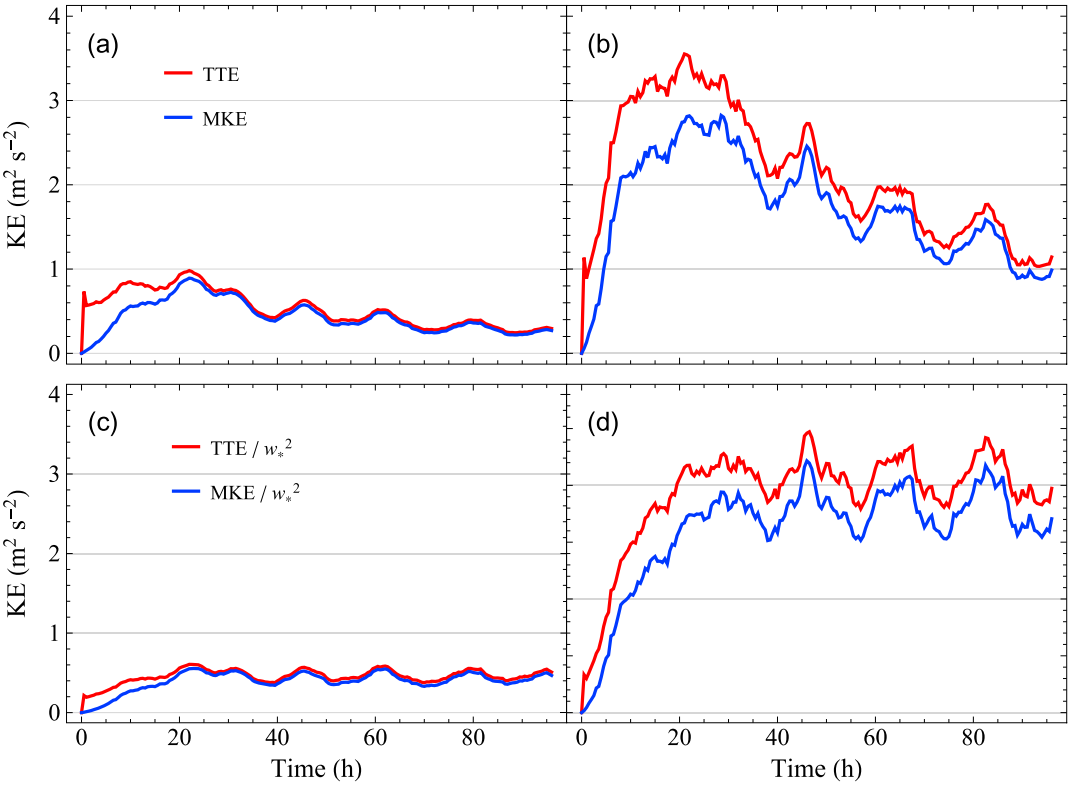

Figure 4. The temporal evolution of domain-averaged kinetic energies. (a and c) Rural area. (b and d) Urban area. Figures 4a and 4b show the original values, while Figures 4c and 4d show the normalized values.

the UHI circulation, the domain averaged u is nearly zero for case A0. Our definition of MKE is thus similar to the volume-averaged turbulence kinetic energy or the domain-averaged perturbed kinetic energy in some previous papers [*Letzel and Raasch*, 2003; *Liu et al*., 2011]. It can be seen in Figures 4a and 4b that TTE and MKE have similar trends. As indicated by equations (4) and (5), MKE represents the energy of the mean flow and is the main contributor to TTE. Figures 4d and 4e show the normalized TTE$/w_*^2$ and MKE$/w_*^2$, where the w_* is the convective velocity scale defined by *Deardorff* [1972]. As can be seen, the normalized TTK and MKE reach a quasi-steady state after a 20 h integration period.

It is also noticed that oscillations are present in Figure 4. Even though the oscillation period is almost the same over urban and rural areas, the amplitude of the oscillation is much larger in urban areas, which is directly correlated with the higher surface heating rate in urban areas. This expected result indicates that the intensity of surface heating plays an important role in controlling the kinetic energy of the atmospheric flow. Meanwhile, it can be also seen that the amplitude of the oscillation becomes smaller as the simulation continues, which probably results from friction from the ground and the entrainment flux, as discussed in previous studies [*Kang*, 2009; *Kang and Lenschow*, 2014; *Letzel and Raasch*, 2003; *Patton et al*., 2005].

To avoid the influence of initial atmospheric conditions, which may be inconsistent with our surface boundary conditions, and to reach a consistent coupled land-atmosphere state, we need an integration period. Considering the above results, it is deemed that the growth rate of PBL height and normalized kinetic energies after 20 h do not change significantly. Given the computational costs of running multiple sets of experiments, in the following sections, the average results from 18 to 20 h are analyzed if not otherwise stated. By focusing on the coupled consistent land-atmosphere state, this approach also allows us to better understand the long-term response of the atmosphere to changes in surface states under such an urban-rural setting.

3.2. The Different Impacts of Dynamics and Thermodynamics Contrasts

In the first set of experiments, the surface temperatures of both urban and rural areas are set to be higher than the initial atmospheric temperature. For cases A, the surface temperature of urban areas is further higher than that of rural areas. For cases B, the momentum roughness length of urban areas is larger than that of rural areas. For cases AB, both the surface temperature and the momentum roughness length in urban areas are larger than their counterparts in rural areas.

Figure 5 shows the distribution of y-averaged (see Figure 1 for the definition of x and y directions) sensible heat flux in the first set of experiments. As expected, the y-averaged sensible heat flux over urban areas is significantly larger that over rural areas, which leads to a distinct UHI circulation and will be demonstrated later in Figure 6. The distribution of sensible heat flux shows a valley shape over urban areas. This is due to the mixing power of turbulence causing the air temperature at the junction fairly uniform over both urban and rural areas. As a result, the abrupt change of surface temperature (or momentum roughness length) occurring at the junction results in an abrupt change of sensible heat flux. From Figure 5a, it can be seen that the urban-rural contrasts of TSK and z_0 have significant but different effects on sensible heat flux. In our simulations, the urban averaged sensible heat flux is 61.4 W m^{-2} in case A0 (A indicates that TSK is higher in urban areas), whereas its counterpart in case B0 is only 14.4 W m^{-2} (B indicates that z_0 is larger in urban areas). The difference in the magnitude of sensible heat flux is related to the magnitude of urban-rural contrasts of TSK (2 K) and z_0 (0.4 m). As can be seen from equations (1) and (2), HFX scales nearly linearly with $(\theta_s - \theta_a)$ but logarithmically with (z/z_0). As a result, changing TSK from 304 to 306 K results in a change of $(\theta_s - \theta_a)$ from 4 to 6 K (note that the initial θ_a is 300 K), namely, by a factor of 1.5. However, a change of z_0 from 0.1 to 0.5 m changes HFX only by a factor of 0.65 assuming $z = 10$ m. From Table 1, we can see that the sensible heat flux is obviously larger with larger TSK (cf., case A0 and case W0), while it is not evident with larger z_0. Interestingly, the frictional velocity u_* is case AB0 (0.335 m s^{-1}) > A0 (0.243) > B0 (0.146) > W0 (0.101). In other words, the larger TSK also significantly enhances the shear stress, which, as shall be seen later, is related to the induced UHI circulations. As a result, the trend in Obukhov length L, which is dominated by the trend in u_*, indicates that W0 is the most unstable case as compared to A0, B0, and AB0.

The geostrophic wind speed plays an important role in modulating the distribution of y-averaged sensible heat flux. As the geostrophic wind speed increases, the friction velocity u_* generally increases and the PBL becomes closer to neutral conditions (except A1 versus A0 and AB1 versus AB0). It is clear from Figure 5b that the valley shape of sensible heat flux in urban area when the geostrophic wind speed is 1 m s^{-1} shifts to the

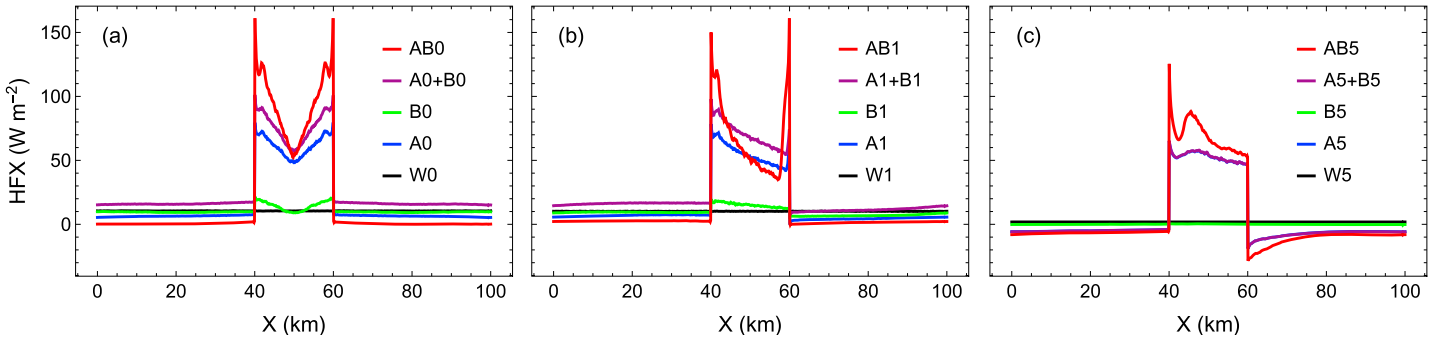

Figure 5. The impacts of urban-rural contrasts of TSK (cases A) and z_0 (cases B) on the *y*-averaged sensible heat flux under the wind speed of (a) 0 m s^{-1}, (b) 1 m s^{-1}, and (c) 5 m s^{-1}.

right (i.e., downwind) as compared to its counterpart in Figure 5a where there is no wind. As a result, this enhances the shear stress on left part of the urban area while reduces the shear stress on the right part of the urban area, which explains why case A1 (and case AB1) has a lower u_* value than A0 (and AB0). When the wind speed is sufficiently large (5 m s^{-1} in Figure 5c), the air temperature over the upwind rural area has an important influence on the sensible heat flux over urban areas that the valley shape almost disappears. According to Figure 5b, even under a same background wind speed, the lowest position of the valley shape of sensible heat flux distribution is not same for different cases. The minimum sensible heat flux in case AB1 occurs at a location closer to the urban center ($x = 50$ km) because of its higher sensible heat flux than in cases A1 and B1, which leads to a stronger UHI circulation. Comparing case B1 to A1 reveals that the impact of urban-rural contrast of z_0 on the sensible heat flux is smaller as compared to the impact of urban-rural

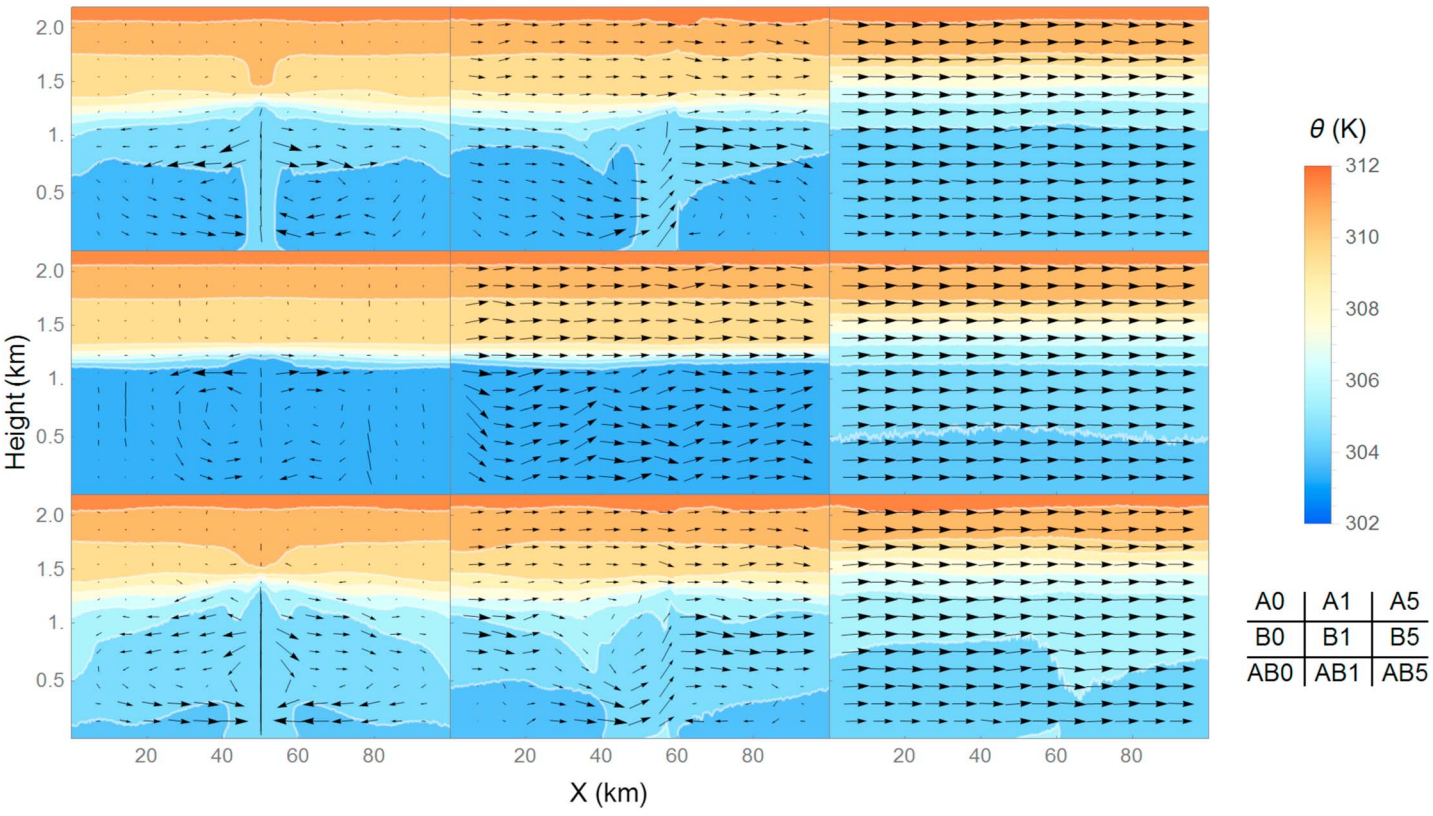

Figure 6. Potential temperature and wind profiles in the first set of experiments. (left column) A geostrophic wind speed of 0 m s^{-1}. (middle column) A geostrophic wind speed of 1 m s^{-1}, and (right column) a geostrophic wind speed of 5 m s^{-1}. (top row) Cases A, (middle row) cases B, and (bottom row) cases C.

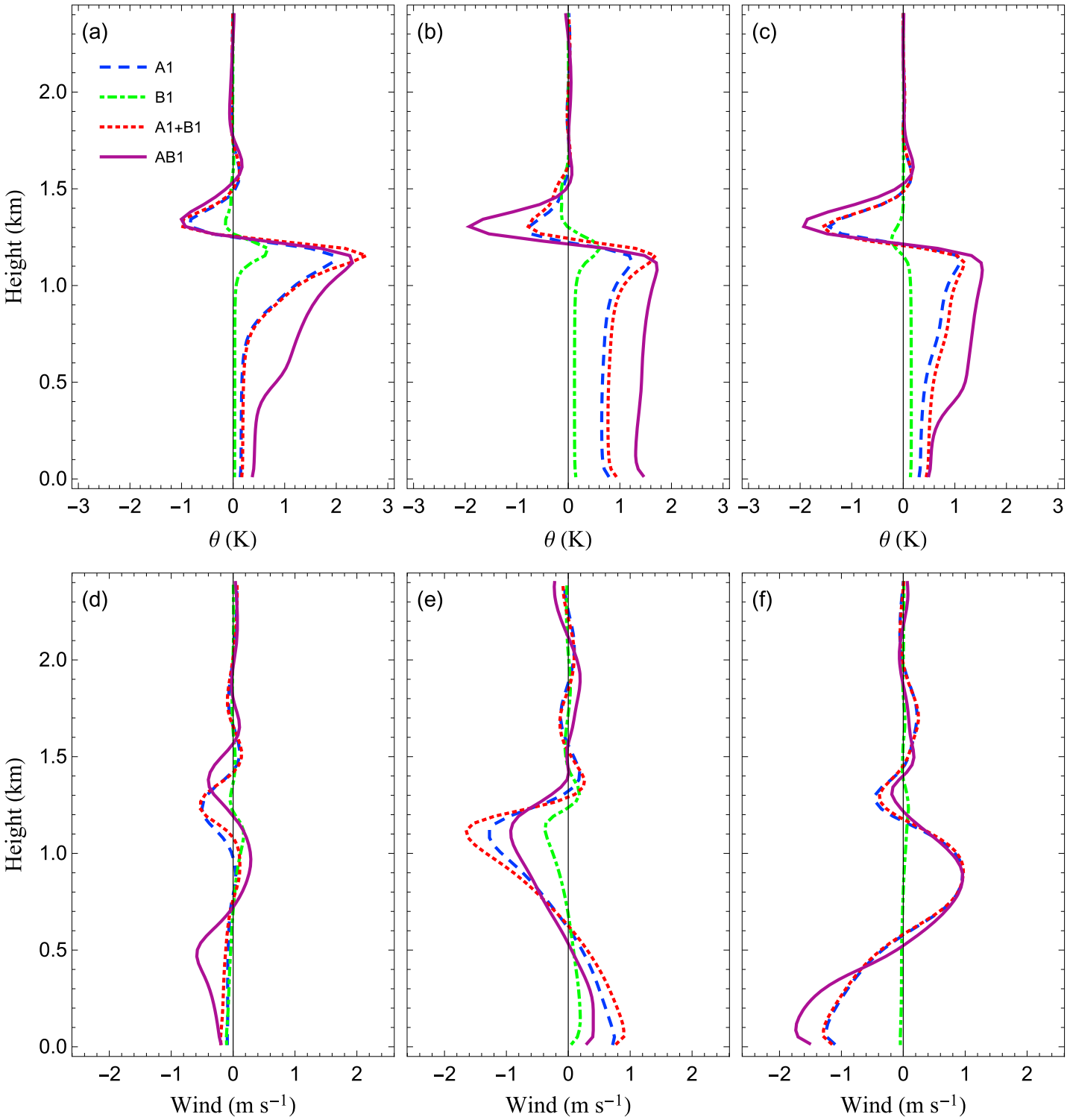

Figure 7. Changes in the *y* averaged potential temperature and wind speed profiles in the first set of experiments when the geostrophic wind speed is 1 m s^{-1}. (a and d) Results from the upwind rural area; (b and e) results from the middle urban area; (c and f) results from the downwind rural area.

contrast of TSK as explained earlier and that the UHI circulation caused by the urban-rural contrast of momentum roughness length is weaker.

It should be noted that the sum of case A0 and case B0 is not identical to the case AB0 as shown in Figure 5a. The sensible heat flux from case AB0 is larger than the sum of case A0 and case B0 over urban areas. This

indicates that the dynamic and thermodynamic characteristics defined here by z_0 and TSK are not independent as expected. For the cases with background wind speed of 1 m s^{-1}, the sum of case A1 and case B1 in the urban center is higher than the caseAB1. This is because the lowest point of the valley shape in the case AB1 is at a different and upwind location as compared to that in the result of A1 + B1, which is further due to the fact that the surface heating rate is stronger in urban areas and the background wind effect is thus relatively weaker in the case AB1 as compared to A1 + B1.

The *y*-averaged vertical distributions of potential temperature and wind in the first set of experiments are shown in Figure 6. It can be seen from cases A0 and B0 that the air rises over urban areas and sinks over rural areas and forms an UHI circulation because of urban-rural contrasts of TSK or z_0. The physical mechanisms, however, differ for these cases. For case A0, the air rises due to a stronger heating rate, while for case B0, the air rises due to the slowdown of air over urban areas, which is further due to a stronger drag force. As a result of this UHI circulation, the lower level wind converges over urban areas and the upper level wind diverges. Quantitatively, in the case A0 the potential temperature in the boundary layer over urban areas is about 1 K higher than that over rural areas, while the difference in case B0 is about 0.3 K. The maximum values of the lower level wind and the upper level wind are 2.4 m s^{-1} and 3.9 m s^{-1}, respectively, in case A0, while they are 1.1 m s^{-1} and 1.7 m s^{-1}, respectively, in case B0. These maximum values all appear at the location near $x = 40$ km and 60 km, which are the edges of urban areas. The vertical wind speed below the inversion layer at the circulation center is also larger in case A0 than in case B0, with a maximum value of 0.45 m s^{-1} and 0.3 m s^{-1} for cases A0 and B0, respectively. Moreover, the case AB0 develops a considerably stronger UHI circulation than both A0 and B0 cases, with a maximum potential temperature difference between urban and rural areas of 1.7 K and a maximum vertical wind speed of 0.68 m s^{-1}.

It should be noted that the location of the circulation center varies in different cases due to the influence of winds. When there is no wind (A0, B0, and AB0), the circulation center is at $x = 50$ km (i.e., the center of urban areas). The UHI circulation in the cases A1, B1, and AB1 is still clearly seen but is moved toward right, or the downwind direction, due to the background wind of 1 m s^{-1}. As the intensity of the UHI circulation increases (AB1 $>$ A1 $>$ B1), the distance of the UHI circulation from the domain center is smaller. When the wind speed is sufficiently large (e.g., for cases A5, B5, and AB5), the UHI circulation is diminished. Specifically, in case A5, the averaged potential temperature in the urban center is 304.4 K as compared to 304.3 K in rural areas and the maximum vertical wind speed at the circulation center is just 0.1 m s^{-1}. This indicate that the wind speed also plays an important role and the UHI circulation is more clearly seen under calm conditions.

Figure 7 shows the differences in the potential temperature and wind speed profiles between different cases and the control case W when the geostrophic wind speed is 1 m s^{-1}. In urban areas, the potential temperature below 1.1 km (within the PBL) is higher than the control case, while the potential temperature above 1.1 km is lower than the control case. The colder anomaly above 1.1 km and the warmer anomaly below 1.1 km create a smaller potential temperature gradient and thus a weaker inversion and facilitates the growth of PBL. It is clear that changes in the potential temperature profiles over rural areas are very different from those in urban areas. In addition, due to the wind, changes in the downwind rural areas are also different from changes in the upwind urban areas. For example, throughout the PBL except near the inversion, changes in the potential temperature over rural areas are nearly an order of magnitude smaller due to a weaker surface heating rate. Changes in the downwind rural area are also larger than changes in the upwind rural area except near the inversion.

Changes in the wind speed show more complex patterns. First, the upwind rural area (Figure 7d) shows small changes of the wind speed, which is again due to the background wind effect that moves the circulation center toward downwind direction. Second, in the urban area (Figure 7e), changes in the wind speed for cases A1 and B1 are negative at the PBL top. The fact that the upper level of urban areas develops a diverging flow makes the wind speed in urban area smaller than the control case. It is also noticed that the differences between case AB1 and W1 are small in urban areas while large in the downwind rural area. From Figure 6 it can be seen that the center of the UHI circulation is almost over the right rural area so the differences in wind speed in urban areas are small while the differences over the downwind rural area are large (Figure 7f). Over the downwind rural area, the increased outward wind speed at 1.1 km and the inward wind speed around 0.1 km are a manifestation of the UHI circulation seen in Figure 6.

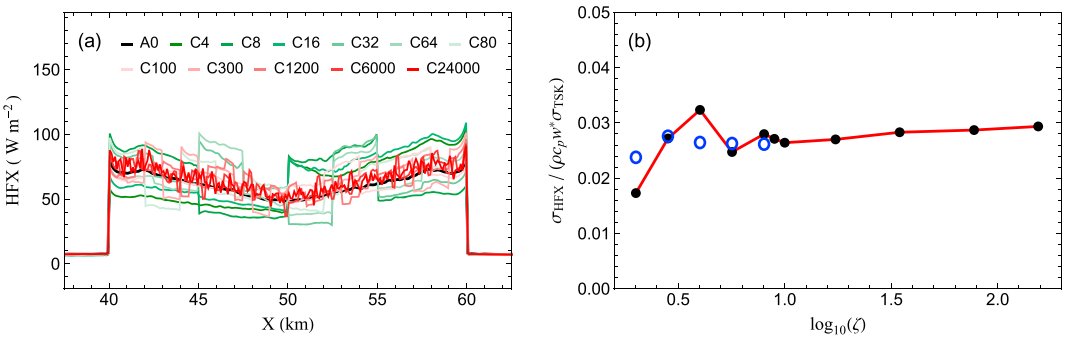

Figure 8. (a) The *y*-averaged sensible heat flux from the second set of experiments; (b) the normalized root-mean-square deviation of sensible heat flux between C cases and the control A0 case.

Comparing the B1 case to A1 case shows that changes in both potential temperature and wind speed are similar but smaller in magnitude, which is consistent with the smaller change in the sensible heat flux in case B1 observed in Figure 5. It is also noted that results from the case AB1 are different from the sum of results from case A1 and B1, which is again consistent with the finding from Figure 5.

3.3. The Impacts of Small-Scale Urban Heterogeneities Within the Context of Large-Scale Urban-Rural Contrast

In the previous section, the UHI circulation induced by urban-rural contrasts of dynamic and thermodynamic characteristics is discussed. In this section, we use results from the second set of experiments to further study the impacts of small-scale urban heterogeneities within the context of large-scale urban-rural contrast, with a specific focus on the importance of surface heterogeneity scale. In the second set of experiments, the urban surface temperature has the same spatial mean as the control case A0 (i.e., 306 K) but varies across different patches. The number of patches increases as the number in the case name increases. It is pointed out here that the large-scale urban-rural contrasts are one-dimensional heterogeneities, but the small-scale heterogeneities examined here are two-dimensional.

Figure 8a shows the spatial distribution of the *y*-averaged sensible heat flux, similar to Figure 5. It can be seen that varying surface temperatures causes different sensible heat fluxes over urban areas but has little influence on sensible heat fluxes over rural areas. The impact on urban sensible heat fluxes varies significantly as the patch size changes. According to Figure 8a, the sensible heat flux distribution becomes more random but closer to the control case result as the heterogeneity scale becomes smaller (or as the case name number becomes larger). Large differences are seen for cases when the heterogeneity scale is large (or when the case name number is small). The maximum difference between different cases and the control case reaches 40 W m^{-2} in the case C64, which is nearly 50% higher than the value in the control case A0.

In order to quantify the effect of these small-scale urban heterogeneities, we use the root-mean-square deviation (σ) between C cases and the control case A0 in terms of sensible heat flux, which is further normalized by the air density, the specific heat capacity c_P, the convective velocity scale w_*, and the standard deviation of the surface temperature in the urban area σ_{TSK}. We also use the following index ζ to represent the relative heterogeneity scale defined as

$$\zeta = \frac{1}{\sqrt{S_{patch}/S_{urban}}} \tag{6}$$

Here s_{patch} is the area of the patch and s_{urban} is the total urban area. When ζ is larger, the heterogeneity scale is smaller (i.e., smaller patches). As can be seen from Figure 8b, when $\log_{10}(\zeta)$ is larger than 1, the normalized root-mean-square deviation of sensible heat flux differences (the black dots connected by the red line) no

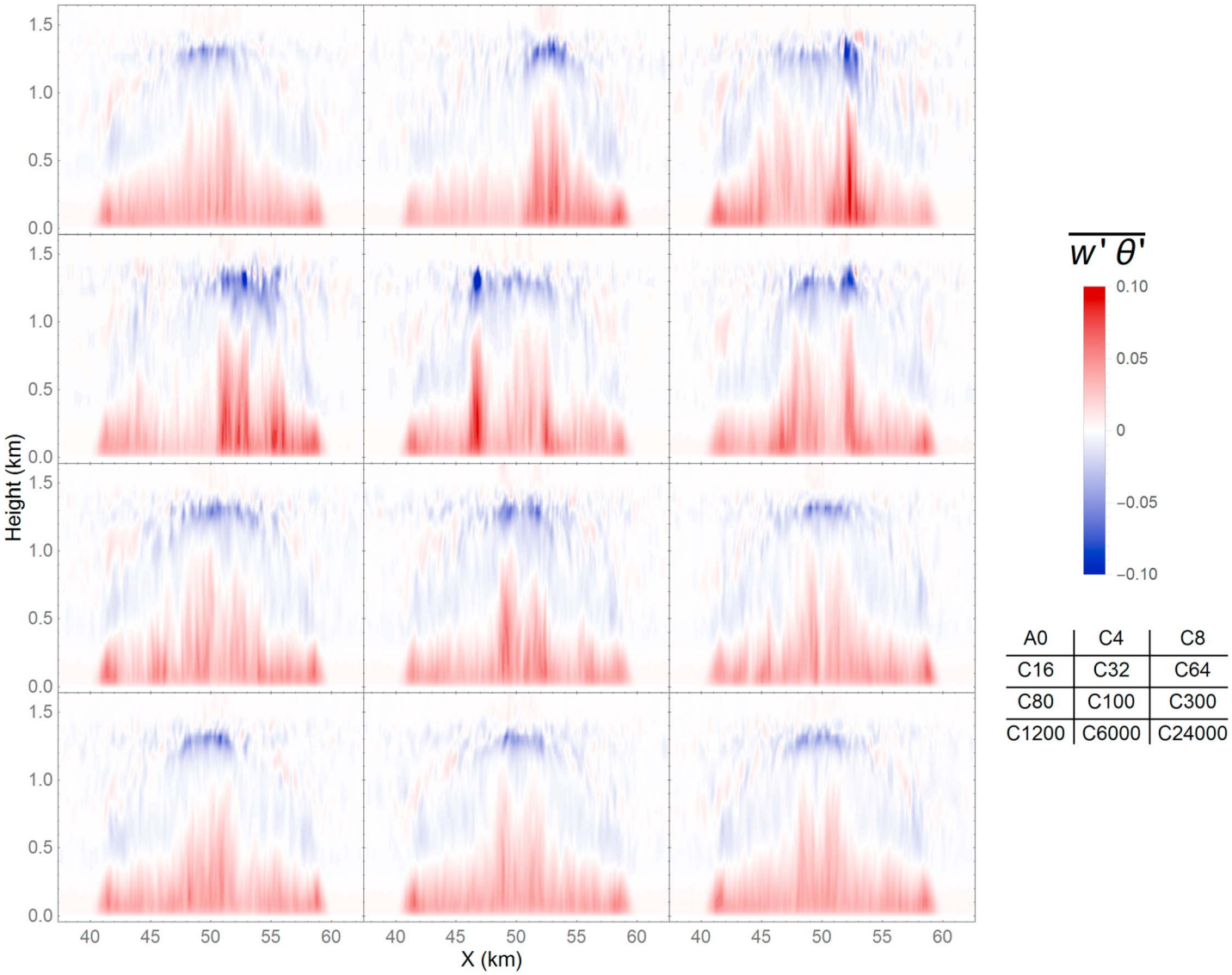

Figure 9. The sensible heat flux over the urban area in the second set of experiments.

longer changes significantly, implying that the effect of small-scale heterogeneities is stabilized. When $\log_{10}(\zeta)$ is smaller than 1, the normalized deviation of sensible heat flux differences is fairly random (despite the fact that the TSK variability is restricted by $\sigma_{TSK} = 1$ K). This implies that when the heterogeneity scale is large, the effect of surface heterogeneity can be large or small depending on the exact TSK value of each patch, which is again randomly selected from a Gaussian distribution in our study.

Some previous studies have proposed the concept of optimal heterogeneity scale at which the impact of surface heterogeneity on kinetic energy maximizes [*Baidya Roy*, 2003; *Patton et al*., 2005; *Van Heerwaarden et al*., 2014]. If the impact of surface heterogeneity is quantified by normalized root-mean-square deviation of the sensible heat flux between the heterogeneous case and the homogeneous case, it appears that $\zeta = 0.6$ would be such optimal heterogeneity scale. In order to verify this result, we reran the large heterogeneous scale cases (C4, C8, C16, C32, and C64) with different but again randomly selected TSK values (described in the section 2.2). The new results, shown as blue circles in Figure 8b, do not seem to support the existence of an optimal heterogeneity scale. The difference between our study and previous studies may be explained by the unique configuration of our experimental design, and also the fact that normalized the root-mean-

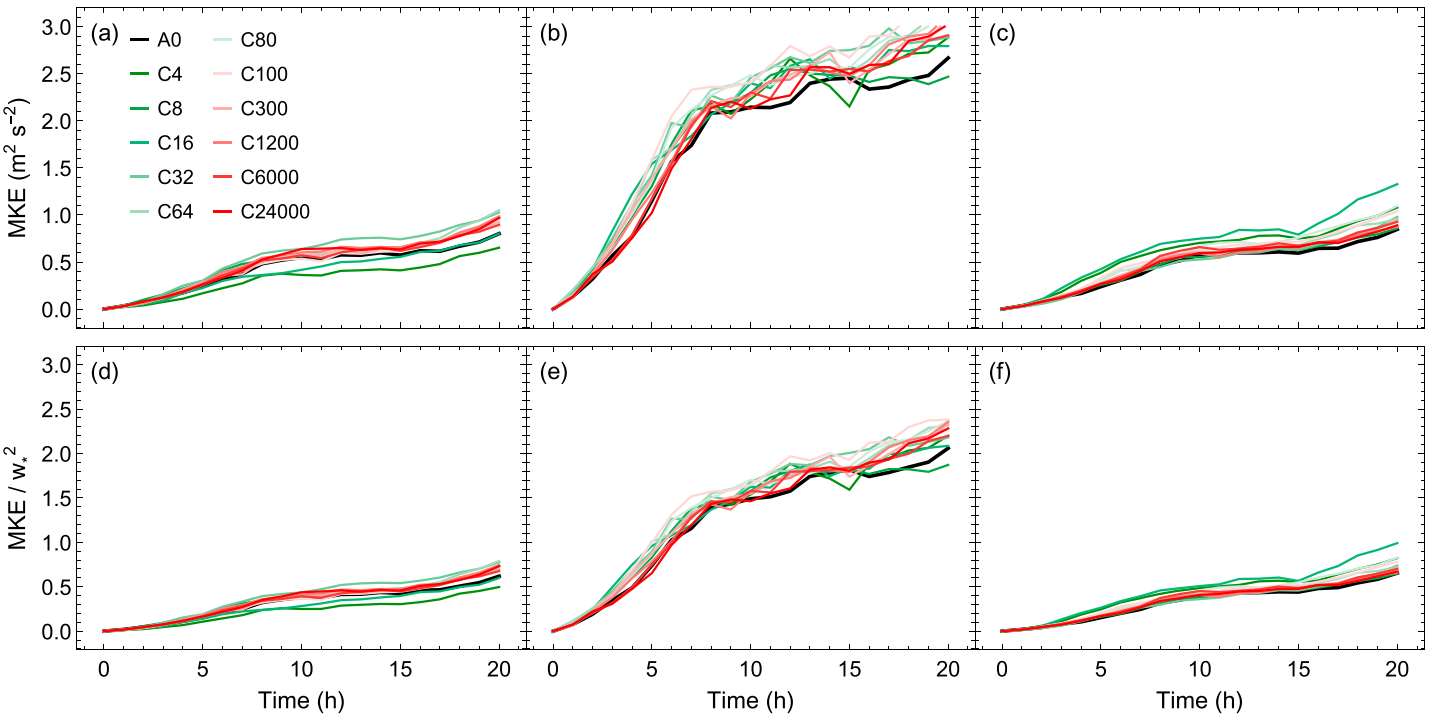

Figure 10. Temporal evolution of mean kinetic energy in the second set of experiments. (a and d) Results in the upwind rural areas; (b and e) results in the middle urban areas; (c and f) results in the downwind rural areas.

square-deviation of sensible heat flux difference is used in our study to diagnose the impact of heterogeneity. The new results, however, reconfirmed that the effect of surface heterogeneity can be affected by the specified TSK values when the heterogeneous scale is large.

Figure 9 further shows the sensible heat flux in the atmosphere (as compared to Figures 5 and 8 showing the surface sensible heat flux) in different cases in the second set of experiments. It can be seen that small-scale urban heterogeneities have an impact on the sensible heat flux, especially near the surface and the inversion layer. It can also be seen that cases with larger heterogeneity scales (such as in cases C4, C8, and C16) more significantly affect the sensible heat flux. Figure 10 shows the temporal evolution of MKE in the second set of experiments, which is computed at 120 m using equation (5). It is interesting to see that the MKE in rural areas, in addition to that in urban areas, is affected by the small-scale heterogeneities in urban areas, especially when the patch size is large. The red lines, which stand for cases with smaller heterogeneity scales, are generally closer to the control homogeneous case (A0), which again implies that results become more similar to those in the homogenous case as the heterogeneity scale reduces. Previous studies have shown that cases with heterogeneous heating will result in an enhanced MKE as compared to cases with homogenous heating under otherwise similar conditions [*Letzel and Raasch*, 2003; *Liu et al*., 2011]. In our study, this seems to be true in general but not for two cases in the upwind rural area, where the MKE in cases C4 and C16 is lower than that in the homogenous case. This is again related to the fact that when the number of patches is small, the exact TSK value of each patch plays an important role. These results indicate that small-scale urban heterogeneities can enhance MKE over the urban area and can also affect the rural MKE especially when the heterogeneity scale is large. When the patch size is large, the exact values of surface characteristics (which in our study is TSK) also matter.

To investigate how the heterogeneity affects the thermal environment, Figure 11 shows the difference in the *y*-averaged vertical distribution of potential temperature (normalized by the $\sigma_{TSK} = 1$ K) between four different C cases (C4, C32, C100, and C6000) and the control case A0. It is clear that the potential temperature over both urban and rural areas has been affected by the heterogeneous surface heating through the UHI

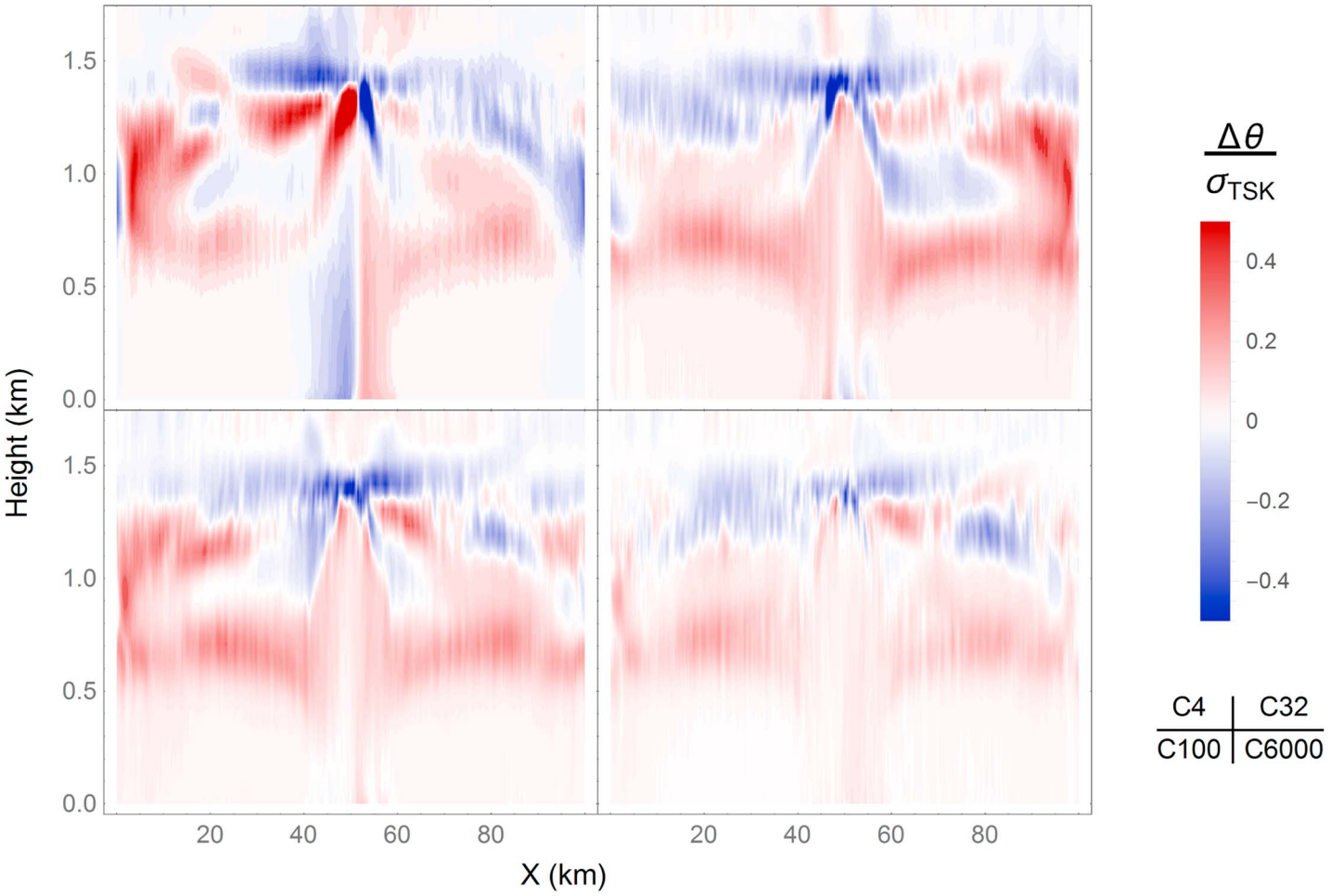

Figure 11. Differences in the *y*-averaged potential temperature between (a) C4, (b) C32, (c) C100, (d) C6000, and the default case A0.

circulation, similar to the MKE. Similar to the effect of urban-rural contrasts, the heterogeneity in urban areas also strongly affects the potential temperature around the inversion, which makes a weaker inversion and favors PBL development as compared to the control case. It can be also found that as the heterogeneity scale decreases, the differences in potential temperature gradually become smaller.

4. Conclusions

In order to understand the impacts of urbanization on regional climate, this study investigates changes in the sensible heat flux, kinetic energy, potential temperature, and wind profiles due to changes in the momentum roughness length and surface temperature by using large eddy simulations with the Weather Research and Forecasting model. In addition, the impacts of small-scale urban heterogeneities within the context of large-scale urban-rural contrast are also studied. The results indicate the following:

1. The urban-rural contrasts in momentum roughness length and surface temperature have significant but different effects on the surface heat flux, the circulation, and the vertical distribution of potential temperature and wind. Changes in momentum roughness length and surface temperature due to urbanization, which represent changes in the dynamic and thermodynamic characteristics, tend to induce a stronger surface heating rate and a weaker inversion layer that favors development of a stronger planetary boundary layer over urban areas. With a low geostrophic wind speed, the induced urban heat island circulation is evident. However, when the geostrophic wind speed is sufficiently large (5 m s^{-1} in our simulations), the urban circulation is diminished, which is consistent with many previous studies.

2. The small-scale surface heterogeneity in terms of surface temperature in urban areas has an important effect on the spatial distribution of sensible heat flux and the vertical profiles of potential temperature. Cases with heterogeneous heating have enhanced kinetic energy over urban areas. Under the influence of the UHI circulation, potential temperatures in both urban and rural areas can be affected by the small-scale heterogeneous surface heating in urban areas. When the urban surface heterogeneity scale is large, the exact surface temperature value of each patch plays an important role. As the heterogeneity scale decreases, the difference from the control case where there is no surface heterogeneity in urban areas becomes smaller.

In conclusion, the study provides insights into the different effects of the dynamic and thermodynamic characteristics of urban surfaces and the often-ignored impacts of small-scale urban heterogeneities in an urban-rural setting. Our study provides a platform for further investigating the impact of mitigation and adaption strategies, which often occur at small-scales. In addition, how the moisture exchange between the land surface and the atmosphere is affected by surface heterogeneity in such urban-rural settings remains an open question. Future work involves examining the coupled heat-water dynamics and the associated impacts on the urban water cycle.

Acknowledgments
This work was supported by the NSFC (51190092 and 51409147), by the China Postdoctoral Science Foundation (2015 T80093), and by the Open Research Fund Program of State key Laboratory of Hydroscience and Engineering (2015-A-02). The simulations were performed on the supercomputing clusters of Tsinghua National Laboratory for Information Science and Technology. X.Z. acknowledges the support from the Tsinghua Fudaoyuan Research Fund. The authors thank the Editor Allison Steiner and the three reviewers for their insightful and constructive comments that significantly improve the quality of this work. The data for this paper are available through request to the corresponding author via sunting@tsinghua.edu.cn.

References

Albertson, J. D., W. P. Kustas, and T. M. Scanlon (2001), Large-eddy simulation over heterogeneous terrain with remotely sensed land surface conditions, *Water Resour. Res.*, *37*(7), 1939–1953, doi:10.1029/2000WR900339.

Arnfield, A. J. (2003), Two decades of urban climate research: A review of turbulence, exchanges of energy and water, and the urban heat island, *Int. J. Climatol.*, *23*(1), 1–26, doi:10.1002/joc.859.

Baidya Roy, S. (2003), A preferred scale for landscape forced mesoscale circulations?, *J. Geophys. Res.*, *108*(D22), 8854, doi:10.1029/2002JD003097.

Basu, S., A. Holtslag, B. Wiel, A. Moene, and G.-J. Steeneveld (2008), An inconvenient "truth" about using sensible heat flux as a surface boundary condition in models under stably stratified regimes, *Acta Geophys.*, *56*(1), 88–99, doi:10.2478/s11600-007-0038-y.

Bou-Zeid, E., C. Meneveau, and M. B. Parlange (2004), Large-eddy simulation of neutral atmospheric boundary layer flow over heterogeneous surfaces: Blending height and effective surface roughness, *Water Resour. Res.*, *40*, W02505, doi:10.1029/2003WR002475.

Bou-Zeid, E., M. B. Parlange, and C. Meneveau (2007), On the parameterization of surface roughness at regional scales, *J. Atmos. Sci.*, *64*(1), 216–227, doi:10.1175/jas3826.1.

Carlson, T. N., and F. E. Boland (1978), Analysis of urban-rural canopy using a surface heat flux/temperature model, *J. Appl. Meteorol.*, *17*(7), 998–1013, doi:10.1175/1520-0450(1978)017<0998:AOURCU>2.0.CO;2.

Chen, F., and J. Dudhia (2001), Coupling an advanced land surface–hydrology model with the Penn State–NCAR MM5 Modeling System. Part I: Model implementation and sensitivity, *Mon. Weather Rev.*, *129*(4), 569–585, doi:10.1175/1520-0493(2001)129<0569:CAALSH>2.0.CO;2.

Deardorff, J. W. (1972), Numerical Investigation of Neutral and Unstable Planetary Boundary Layers, *J. Atmos. Sci.*, *29*(1), 91–115, doi:10.1175/1520-0469(1972)029<0091:NIONAU>2.0.CO;2.

Deardorff, J. W. (1980), Stratocumulus-capped mixed layers derived from a three-dimensional model, *Boundary-Layer Meteorol.*, *18*(4), 495–527, doi:10.1007/BF00119502.

Gibbs, J. A., E. Fedorovich, and A. Shapiro (2014), Revisiting surface heat-flux and temperature boundary conditions in models of stably stratified boundary-layer flows, *Boundary-Layer Meteorol.*, *154*(2), 171–187, doi:10.1007/s10546-014-9970-y.

Grimm, N. B., S. H. Faeth, N. E. Golubiewski, C. L. Redman, J. Wu, X. Bai, and J. M. Briggs (2008), Global change and the ecology of cities, *Science*, *319*(5864), 756–760, doi:10.1126/science.1150195.

Grimmond, S. (2007), Urbanization and global environmental change: Local effects of urban warming, *Geogr. J.*, *173*, 83–88, doi:10.1111/j.1475-4959.2007.232_3.x.

Hidalgo, J., V. Masson, and C. Pigeon (2008a), Urban-breeze circulation during the CAPITOUL experiment: Numerical simulations, *Meteorol. Atmos. Phys.*, *102*(3-4), 243–262, doi:10.1007/s00703-008-0345-0.

Hidalgo, J., G. Pigeon, and V. Masson (2008b), Urban-breeze circulation during the CAPITOUL experiment: Observational data analysis approach, *Meteorol. Atmos. Phys.*, *102*(3-4), 223–241, doi:10.1007/s00703-008-0329-0.

Holtslag, A. A. M., G. J. Steeneveld, and B. J. H. van de Wiel (2007), Role of land-surface temperature feedback on model performance for the stable boundary layer, *Boundary-Layer Meteorol.*, *125*(2), 361–376, doi:10.1007/s10546-007-9214-5.

Huang, H. Y., and S. A. Margulis (2010), Evaluation of a fully coupled large-eddy simulation-land surface model and its diagnosis of land-atmosphere feedback, *Water Resour. Res.*, *46*, W06512, doi:10.1029/2009WR008232.

Kang, S. L. (2009), Temporal oscillations in the convective boundary layer forced by mesoscale surface heat-flux variations, *Boundary-Layer Meteorol.*, *132*(1), 59–81, doi:10.1007/s10546-009-9391-5.

Kang, S. L., and D. H. Lenschow (2014), Temporal evolution of low-level winds induced by two-dimensional mesoscale surface heat-flux heterogeneity, *Boundary-Layer Meteorol.*, *151*(3), 501–529, doi:10.1007/s10546-014-9912-8.

Lee, X., et al. (2011), Observed increase in local cooling effect of deforestation at higher latitudes, *Nature*, *479*(7373), 384–387, doi:10.1038/nature10588.

Letzel, M. O., and S. Raasch (2003), Large eddy simulation of thermally induced oscillations in the convective boundary layer, *J. Atmos. Sci.*, *60*(18), 2328–2341, doi:10.1175/1520-0469(2003)060<2328:Lesoti>2.0.Co;2.

Li, D., and E. Bou-Zeid (2013), Synergistic interactions between urban heat islands and heat waves: The impact in cities is larger than the sum of its parts*, *J. Appl. Meteorol. Climatol.*, *52*(9), 2051–2064, doi:10.1175/JAMC-D-13-02.1.

Li, D., T. Sun, M. Liu, L. Yang, L. Wang, and Z. Gao (2015), Contrasting responses of urban and rural surface energy budgets to heat waves explain synergies between urban heat islands and heat waves, *Environ. Res. Lett.*, *10*(5), 054009, doi:10.1088/1748-9326/10/5/054009.

Li, D., T. Sun, M. Liu, L. Wang, and Z. Gao (2016), Changes in wind speed under heat waves enhance urban heat islands in Beijing metropolitan area, *J. Appl. Meteorol. Climatol.*, doi:10.1175/JAMC-D-16-0102.1.

Liu, G., J. Sun, and L. Yin (2011), Turbulence characteristics of the shear-free convective boundary layer driven by heterogeneous surface heating, *Boundary-Layer Meteorol.*, *140*(1), 57–71, doi:10.1007/s10546-011-9591-7.

Lowry, W. P. (1998), Urban effects on precipitation amount, *Prog. Phys. Geogr.*, *22*(4), 477–520, doi:10.1177/030913339802200403.

Miao, S. G., F. Chen, Q. C. Li, and S. Y. Fan (2011), Impacts of urban processes and urbanization on summer precipitation: A case study of heavy rainfall in Beijing on 1 August 2006, *J. Appl. Meteorol. Climatol.*, *50*(4), 806–825, doi:10.1175/2010jamc2513.1.

Miller, N. E., and R. Stoll (2013), Surface heterogeneity effects on regional-scale fluxes in the stable boundary layer: Aerodynamic roughness length transitions, *Boundary-Layer Meteorol.*, *149*(2), 277–301, doi:10.1007/s10546-013-9839-5.

Moeng, C. H., J. Dudhia, J. Klemp, and P. Sullivan (2007), Examining two-way grid nesting for large eddy simulation of the PBL using the WRF model, *Mon. Weather Rev.*, *135*(6), 2295–2311, doi:10.1175/mwr3406.1.

Monin, A. S., and A. Obukhov (1954), Basic laws of turbulent mixing in the surface layer of the atmosphere, *Contrib. Geophys. Inst. Acad. Sci. USSR*, *151*, 163–187.

Oke, T. R. (1982), The energetic basis of the urban heat-island, *Q. J. R. Meteorol. Soc.*, *108*(455), 1–24, doi:10.1002/qj.49710845502.

Patton, E. G., P. P. Sullivan, and C. H. Moeng (2005), The influence of idealized heterogeneity on wet and dry planetary boundary layers coupled to the land surface, *J. Atmos. Sci.*, *62*(7), 2078–2097, doi:10.1175/Jas3465.1.

Rizwan, A. M., Y. C. L. Dennis, and C. H. Liu (2008), A review on the generation, determination and mitigation of urban heat island, *J. Environ. Sci.-China*, *20*(1), 120–128, doi:10.1016/S1001-0742(08)60019-4.

Ryu, Y. H., and J. J. Baik (2013), Daytime local circulations and their interactions in the Seoul metropolitan area, *J. Appl. Meteorol. Climatol.*, *52*(4), 784–801, doi:10.1175/Jamc-D-12-0157.1.

Ryu, Y. H., J. J. Baik, and J. Y. Han (2013), Daytime urban breeze circulation and its interaction with convective cells, *Q. J. R. Meteorol. Soc.*, *139*(671), 401–413, doi:10.1002/qj.1973.

Schneider, A., M. A. Friedl, and D. Potere (2009), A new map of global urban extent from MODIS satellite data, *Environ. Res. Lett.*, *4*(4), 044003, doi:10.1088/1748-9326/4/4/044003.

Shepherd, J. M. (2005), A review of current investigations of urban-induced rainfall and recommendations for the future, *Earth Interact.*, *9*(12), 1–27, doi:10.1175/EI156.1.

Stoll, R., and F. Porté-Agel (2006), Dynamic subgrid-scale models for momentum and scalar fluxes in large-eddy simulations of neutrally stratified atmospheric boundary layers over heterogeneous terrain, *Water Resour. Res.*, *42*, W01409, doi:10.1029/2005WR003989.

Stoll, R., and F. Porté-Agel (2009), Surface heterogeneity effects on regional-scale fluxes in stable boundary layers: Surface temperature transitions, *J. Atmos. Sci.*, *66*(2), 412–431, doi:10.1175/2008JAS2668.1.

Stull, R. B. (1988), *An Introduction to Boundary Layer Meteorology*, Springer Science & Business Media, Dordrecht, Netherlands.

Talbot, C., E. Bou-Zeid, and J. Smith (2012), Nested mesoscale large-eddy simulations with WRF: Performance in real test cases, *J. Hydrometeorol.*, *13*(5), 1421–1441, doi:10.1175/JHM-D-11-048.1.

United Nations, Department of Economic and Social Affairs, Population Division (2014), World urbanization prospects: The 2014 revision Highlights (ST/ESA/SER.A/352).

Van Heerwaarden, C. C., and J. P. Mellado (2016), Growth and decay of a convective boundary layer over a surface with a constant temperature, *J. Atmos. Sci.*, *73*(5), 2165–2177, doi:10.1175/JAS-D-15-0315.1.

Van Heerwaarden, C. C., J. P. Mellado, and A. De Lozar (2014), Scaling laws for the heterogeneously heated free convective boundary layer, *J. Atmos. Sci.*, *71*(11), 3975–4000, doi:10.1175/jas-d-13-0383.1.

Wang, L. L., D. Li, Z. Q. Gao, T. Sun, X. F. Guo, and E. Bou-Zeid (2014), Turbulent transport of momentum and scalars above an urban canopy, *Boundary-Layer Meteorol.*, *150*, 485–511, doi:10.1007/s10546-013-9877-z.

Wang, W. (2009), The influence of thermally-induced mesoscale circulations on turbulence statistics over an idealized urban area under a zero background wind, *Boundary-Layer Meteorol.*, *131*(3), 403–423, doi:10.1007/s10546-009-9378-2.

Wood, C. R., A. Lacser, J. F. Barlow, A. Padhra, S. E. Belcher, E. Nemitz, C. Helfter, D. Famulari, and C. S. B. Grimmond (2010), Turbulent flow at 190 m height above london during 2006–2008: A climatology and the applicability of similarity theory, *Boundary-Layer Meteorol.*, *137*(1), 77–96, doi:10.1007/s10546-010-9516-x.

Yamaguchi, T., and G. Feingold (2012), Technical note: Large-eddy simulation of cloudy boundary layer with the Advanced Research WRF model, *J. Adv. Model. Earth Syst.*, *4*, M09003, doi:10.1029/2012MS000164.

Yang, L., J. A. Smith, M. L. Baeck, E. Bou-Zeid, S. M. Jessup, F. Tian, and H. Hu (2014), Impact of urbanization on heavy convective precipitation under strong large-scale forcing: A case study over the Milwaukee–Lake Michigan region, *J. Hydrometeorol.*, *15*(1), 261–278, doi:10.1175/jhm-d-13-020.1.

Zhang, N., X. Y. Wang, and Z. Peng (2014), Large-eddy simulation of mesoscale circulations forced by inhomogeneous urban heat island, *Boundary-Layer Meteorol.*, *151*(1), 179–194, doi:10.1007/s10546-013-9879-x.

Zhao, L., X. Lee, R. B. Smith, and K. Oleson (2014), Strong contributions of local background climate to urban heat islands, *Nature*, *511*(7508), 216–219, doi:10.1038/nature13462.